


Configuration of a Nanometric Positioning Robot

Jaime Fernando Cárdenas-García^{1, a} 

Recibido: 20/03/2021

Aceptado: 15/05/2021

Publicado: 01/07/2021

Citar como:

Cárdenas-García, J. (2021). Configuration of a Nanometric Positioning Robot. *Veritas & Research*, 3(1), 60-72.

Abstract

The use of a circular-wedge link pair as a manipulator joint allows for versatility and flexibility in positioning. In particular, its use allows for repeatable, precise, and versatile alignment of mechanical components and has the potential for the configuration and development of adaptable serpentine robots. This paper explores the feasibility of using macrometric circular-wedge links to attain nanometric capable positioners. The forward and inverse kinematics of these positioners configured with two macroscopic circular-wedge links is described. The results show that the workspace defined by these rotationally constrained positioners is essentially planar in nature. The achievable planar range of motion is three orders of magnitude greater than the nanometric motion in the out-of-plane direction. This novel positioner has the potential to satisfy the need for nanometric capable positioning and motion where accuracy, repeatability and versatility are required.

Keywords: *Circular-wedge; serpentine robots; nano-metric capable positioner*

Configuración de un Posicionador Robótico Nanométrico

Resumen

El uso de un par de cuñas-circulares como una articulación de un manipulador permite lograr versatilidad y flexibilidad en posicionamiento. En particular, su uso permite lograr la alineación de componentes mecánicos con repetitividad, precisión y versatilidad, teniendo el potencial para la configuración y desarrollo de robots serpentinados adaptables. Este artículo explora la factibilidad de usar cuñas circulares macrométricas articuladas para obtener posicionadores capaces de movimientos nanométricos. Se describe la cinemática directa e inversa de estos posicionadores con dos cuñas circulares. Los resultados demuestran que el espacio de trabajo definidos por estos posicionadores constreñidos rotacionalmente es esencialmente plano. El movimiento realizable en el plano es tres órdenes de magnitud mayor, que el movimiento nanométrico en la dirección fuera del plano. Este novedoso posicionador tiene el potencial de satisfacer las necesidades para posicionamiento nanométrico y movimiento en donde se requiere precisión, repetitividad y versatilidad.

Palabras clave: *Cuña-circular; robots serpentinados; posicionador nanométrico*

¹ Contact: jfcg@umbc.edu

Configuração de um robô de posicionamento nanométrico

Resumo

O uso de um par de cunhas circulares como uma junta de uma alça permite versatilidade e flexibilidade no posicionamento. Em particular, seu uso permite alcançar o alinhamento de componentes mecânicos com repetitividade, precisão e versatilidade, tendo o potencial para a configuração e desenvolvimento de robôs serpentinados adaptativos. Este artigo explora a viabilidade do uso de cunhas circulares macrométricas articuladas para obter posicionadores capazes de movimentos nanométricos. Descreve a cinemática direta e inversa de posicionadores com duas cunhas circulares. Os resultados mostram que o espaço de trabalho definido por esses posicionadores com restrição rotativa é essencialmente plano. O movimento executável no plano é três ordens de magnitude maior, do que o movimento nanométrico fora do plano. Este posicionador inovador tem o potencial de atender às necessidades de posicionamento e movimento nanométricos onde precisão, repetibilidade e versatilidade são necessárias.

Palavras chave: Cunha circular; robôs serpentinados; posicionamento nanométrico

Introduction and Objectives

The use of circular-wedge links in a remotely controllable actuator system (Harwood 1973) is known. Also, previous work by the author shows that the use of a duplicate pair of dissimilar wedged discs to achieve alignment of surfaces is an approach that satisfies the need for repeatable, accurate, precise, versatile and inexpensive alignment of mechanical components (Cardenas-Garcia, Suryanarayan, and Ingalls 1999). A natural extension is to use a large number of circular-wedge links to structure a highly versatile and flexible serpentine robot (Cardenas-Garcia and Preidikman 2005). Numerous applications for serpentine robots

exist in space-based maintenance; inspections of enclosed areas which are difficult to examine requiring enhanced flexibility and reachability, especially in convoluted environments; search and rescue operations; exploring rough terrain; swimming in contaminated water; and manipulation in places too dangerous for humans. These serpentine structures are robust to mechanical failure if designed to be modular and highly redundant (Hirose 1993; McKerrow 1991). The main objective of this paper is to explore the feasibility of using macro-scale circular-wedge links to achieve nano-metric positioning.

Theoretical Background

This section outlines the forward kinematics of the positioner by means of homogenous transformations (Bejczy 1975; Denavit and Hartenberg 1955; Gutkowski and Kinzel 1995) and the inverse kinematics of a two-link positioner by an algebraic approach (Kucuk and Bingul 2006).

The Basic Assembly Element: The Forward Kinematics of the Circular-Wedge Link

Figure 1 shows a single circular-wedge link and the associated coordinate systems. Three different coordinate systems are identified in order to transfer the local description of vector P_L in coordinate system (x_2, y_2, z_2) to the global coordinate system (x, y, z) described by vector P_G . In equation form,

$$P_G = P_0 + P_L \quad (1)$$

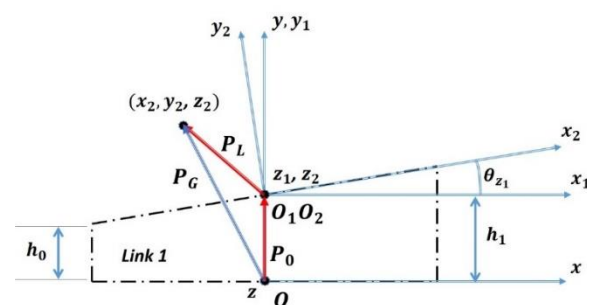


Figure 1. The Coordinate Systems Associated with a Single Circular-wedge Link

What this requires is that several homogeneous transformations be performed on the local vector \mathbf{P}_L to arrive at the global vector \mathbf{P}_G , i.e., the forward kinematics for a single circular-wedge link is given by,

$$\mathbf{P}_G = R[\theta_{y_1}]T[h_1]R[\theta_{z_1}]\mathbf{P}_L \quad (2)$$

where $R[\theta_{y_1}]$ represents the homogeneous transformation for rotation about the y-axis, which is used to rotate *Link 1* about said axis; $T[h_1]$ the homogeneous transformation for translation along the y₁-axis, which is used to account for the thickness of *Link 1* at its center; and $R[\theta_{z_1}]$ is the homogeneous transformation for rotation about the z₁-z₂-axis, which is used to account for the wedge angle inclination of *Link 1*. These homogeneous transformations take the form for *Link 1* of the [4 x 4] matrices defined as follows:

$$R[\theta_{z_1}] = \begin{bmatrix} c\theta_{z_1} & -s\theta_{z_1} & 0 & 0 \\ s\theta_{z_1} & c\theta_{z_1} & 0 & 0 \\ 0 & 0 & 1 & 0 \\ 0 & 0 & 0 & 1 \end{bmatrix} \quad (3a)$$

$$T[h_1] = \begin{bmatrix} 1 & 0 & 0 & 0 \\ 0 & 1 & 0 & h_1 \\ 0 & 0 & 1 & 0 \\ 0 & 0 & 0 & 1 \end{bmatrix} \quad (3b)$$

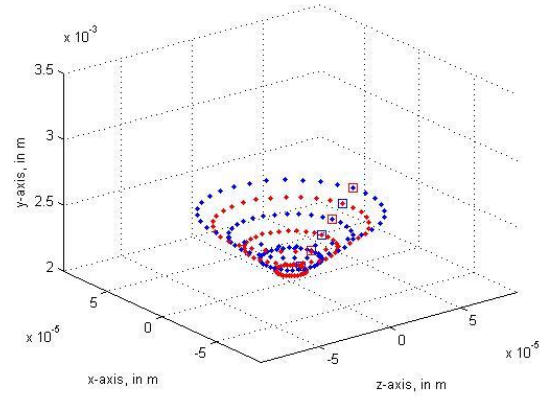
$$R[\theta_{y_1}] = \begin{bmatrix} c\theta_{y_1} & 0 & s\theta_{y_1} & 0 \\ 0 & 1 & 0 & 0 \\ -s\theta_{y_1} & 0 & c\theta_{y_1} & 0 \\ 0 & 0 & 0 & 1 \end{bmatrix} \quad (3c)$$

Note that the sine and cosine of the alluded angles are represented in abbreviated notation as $s\theta_{z_1}$, $s\theta_{y_1}$ and $c\theta_{z_1}$, $c\theta_{y_1}$, respectively. Additionally, the translational distance h_1 is the vertical distance that separates the $O(x, y, z)$ from the $O_1(x_1, y_1, z_1)$ - $O_2(x_2, y_2, z_2)$ set of axes. If the radius of the circumference that defines the bottom surface of *Link 1* is R , then the distance h_1 takes the form

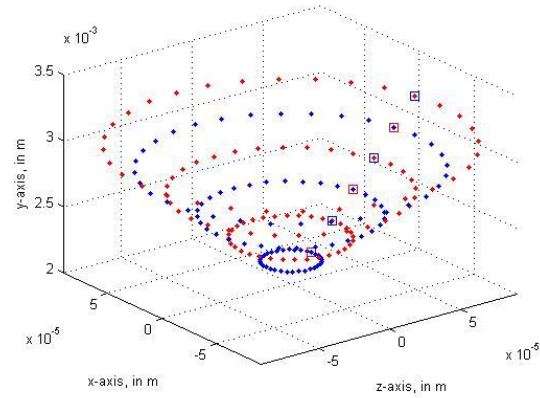
$$h_1 = (h_0)_1 + R \tan[\theta_{z_1}] \quad (4)$$

where $(h_0)_1$ is the thickness of the circular-wedge link at its narrowest, and θ_{z_1} is the circular-wedge link

angle. Additionally, for the geometry shown in Figure 1, $\mathbf{P}_L = \{P_x \ P_y \ P_z \ 1\}^T$ with respect to the local $O_2(x_2, y_2, z_2)$ -axis.



2(a) Increments of 0.5-degrees



2(b) Increments of 1.0-degrees

Figure 2. Trajectory of a Point $\mathbf{P}_L = \{0 \ 1E-3 \ 0 \ 1\}^T$ m for a Single Circular-wedge Link System

Figures 2(a) and 2(b) show the 5-bit or 32-point circular trajectory, for a full rotation of a circular-wedge link ($0 \leq \theta_{y_1} \leq 360 \text{ deg}$), of the tip of \mathbf{P}_L with local coordinates $(0, 1E-3, 0) \text{ m}$ in the Global $O(x, y, z)$ coordinate system, for the single circular-wedge link with dimensions $R = 10E-3 \text{ m}$ and $(h_0)_1 = 1E-3 \text{ m}$ shown in Figure 1.

Figure 2(a) shows the variation of the trajectory for five wedge angle increments of $\theta_{z_1} = 0.5 \text{ deg}$, starting at a value of 0.5 deg . Figure 2(b) shows the variation of the trajectory for five wedge angle increments of $\theta_{z_1} = 1.0 \text{ deg}$, starting at a value of 1.0 deg . An overlapping square symbol shows the position at which the motion of the trajectory begins, in each case. In effect, Figures 2(a) and 2(b) show the comparison of the motion that is achievable by 12 different circular-wedge links reflecting different wedge angles. Since the limits of

the x, y- and z-axes of both Figures are the same, there are common trajectories at values of $\theta_{z_1} = 1.0, 2.0$ and 3.0 deg .

Each circular trajectory depicted in Figures 2(a) and 2(b) is represented by 5-bit or 32-discrete points to simulate the use of a stepper motor to repeatedly access the locations shown in the graph, for each of the represented circular-wedge links. Using stepper motors allows for precise positioning and repeatability of movement since good stepper motors have an accuracy of 3 to 5% of a step and this error is non-cumulative from one step to the next². The tip of P_L for $\theta_{z_1} = 1.0 \text{ deg}$ describes a circular trajectory with a radius of about $1.7452E-5 \text{ m}$ at a height of $2.1744E-3 \text{ m}$. The separation between points is $3.2740E-06 \text{ m}$, which shows the potential for achieving nanometric positioning, i.e., an 8-bit or 256-step per revolution stepper motor achieves a separation between points of $4.2805E-7 \text{ m}$.

The Forward Kinematics of the Double Circular-Wedge Link System

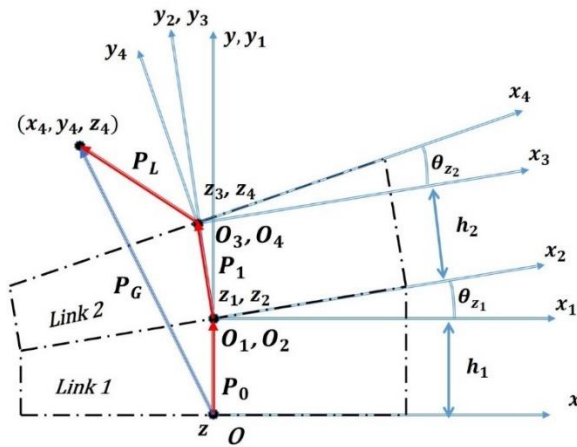


Figure 3. The Coordinate Systems Associated with Two Circular-wedge Links

Figure 3 show the configuration associated with a system of two circular-wedge links, which may or may not be duplicates. The full description of the $\{4 \times 1\}$ global vector P_G which defines the forward kinematics of the system using two circular-wedge links is given by,

$$P_G = R[\theta_{y_1}]T[h_1]R[\theta_{z_1}]R[\theta_{y_2}]T[h_2]R[\theta_{z_2}]P_L \quad (5)$$

The homogeneous transformations associated with Link 2 take the form

$$R[\theta_{z_2}] = \begin{bmatrix} c\theta_{z_2} & -s\theta_{z_2} & 0 & 0 \\ s\theta_{z_2} & c\theta_{z_2} & 0 & 0 \\ 0 & 0 & 1 & 0 \\ 0 & 0 & 0 & 1 \end{bmatrix} \quad (6a)$$

$$T[h_2] = \begin{bmatrix} 1 & 0 & 0 & 0 \\ 0 & 1 & 0 & h_2 \\ 0 & 0 & 1 & 0 \\ 0 & 0 & 0 & 1 \end{bmatrix} \quad (6b)$$

$$R[\theta_{y_2}] = \begin{bmatrix} c\theta_{y_2} & 0 & s\theta_{y_2} & 0 \\ 0 & 1 & 0 & 0 \\ -s\theta_{y_2} & 0 & c\theta_{y_2} & 0 \\ 0 & 0 & 0 & 1 \end{bmatrix} \quad (6c)$$

It is possible to show that by changing the pertinent variables, e.g., setting $(h_0)_1 = 0 \text{ m}$; $\theta_{z_1} = 0.0 \text{ deg}$, or alternatively $(h_0)_2 = 0 \text{ m}$; $\theta_{z_2} = 0.0 \text{ deg}$, you eliminate either the bottom (Link 1) or top (Link 2) circular-wedge link, respectively, to reproduce a single wedge system, and corroborate the calculations performed and shown in Figures 2(a) and 2(b).

Assuming a duplicate circular-wedge link with the same characteristics as the first, it is possible to examine different trajectories that the tip of P_L defined in local coordinates as $P_L = \{0 \text{ L } 0 \text{ 1}\}^T = \{0 \text{ 1E-3 } 0 \text{ 1}\}^T \text{ m}$ describes. Figures 4(a)-4(d) represent the trajectories that the tip of P_L follows depending on the motion of the circular-wedge links, using diagrams whose axes are represented in different scales. Similarly, an overlapping square symbol shows the position at which the motion of the trajectory begins, in each case.

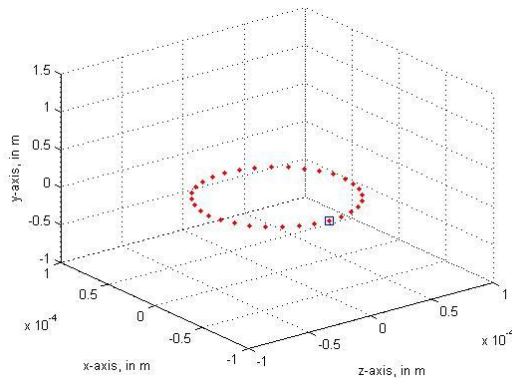
Figure 4(a) shows the resulting trajectory for the 5-bit or 32-step stepping motion of only Link 1 (Bottom), with Link 2 (Top) held motionless. The result is a circular trajectory of the tip of P_L . Figure 4(b) shows the resulting trajectory for the 5-bit or 32-step stepping motion of only Link 2 (Top), with Link 1 (Bottom) held motionless. As expected, the circular trajectory of the tip of P_L lies on a plane at an angle (equivalent to the circular-wedge angle $\theta_{z_2} = 1.0 \text{ deg}$) to the xz-plane.

Figure 4(c) shows the resulting trajectory for the 5-bit or 32-step stepping motion of Link 2 (Top), with the 2-bit or 4-step stepping motion of Link 1 (Bottom). The motion of Link 1 (Bottom) allows the creation of the four (2-bit) distinct circles whose shape is defined by the motion of Link 2 (Top) and corresponds to the 5-bit or 32-step stepping motion of said Link 2 (Top). Figure

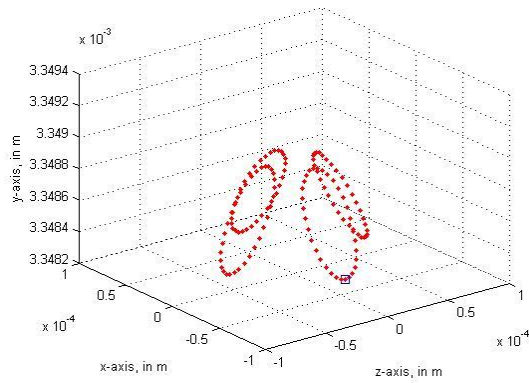
² http://www.omega.com/prodinfo/stepper_motors.html; Accessed: March 19, 2021.

4(d) shows a similar result as that of Figure 4(c), except that *Link 1* (Bottom) undergoes a 3-bit or 8-step stepping motion.

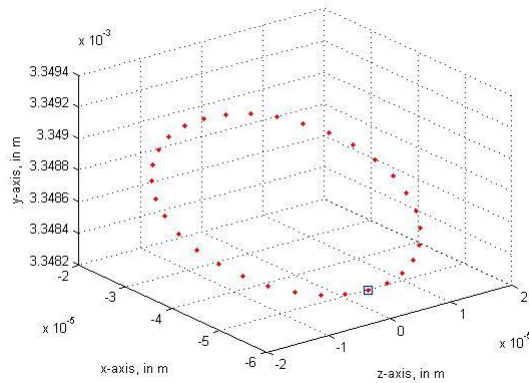
What is common to Figures 4(b)-4(d) is that *Link 1* (Bottom) undergoes a different number of steps, i.e., 0-bit, 2-bit and 3-bit, respectively. The vertical motion per revolution of $6.0917E-7$ m along the y-axis remains the same for all of these figures, while the reach in the xz-plane changes as the number of steps of *Link 1* (Bottom) changes. Figure 5 is a plot of the sinusoidal variation of the in-plane displacements and the out-of-plane displacements shown in Figure 4(b). The in-plane displacements, in the x- (green line) and z- (red line) directions, are plotted using the vertical reference axis on the right of the plot. The out-of-plane displacements, in the y- direction, are plotted using the vertical reference axis on the left of the plot. The reference point for these displacements is the square blue marker symbol (shown at the lowest of the red dot marker symbols) in Figure 4(b) that define the path of the tip trajectories of P_L in the global x-y-z frame of reference. The path of x-displacements, in Figure 5, has been shifted-up by an amount equal to the minimum value of x-displacements added to the average value of x-displacements. This is done so as to have the variation in x-displacements be centered at zero. The x- and z-displacements are 90-degrees out of phase, while the y- and z- displacements are in phase.



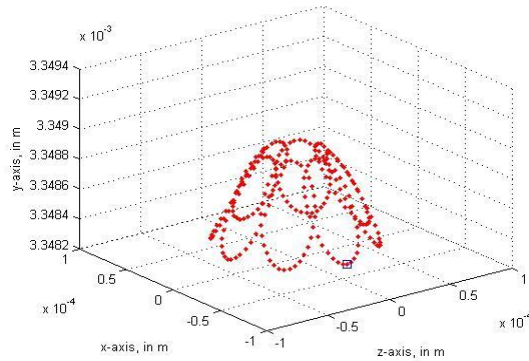
4(a) Link 1 = 2^5 ; Link 2 = 2^0



4(c) Link 1 = 2^2 ; Link 2 = 2^5



4(b) Link 1 = 2^0 ; Link 2 = 2^5



4(d) Link 1 = 2^3 ; Link 2 = 2^5

Figure 4. *Double Circular-wedge Link System Trajectory of a Point $P_L = \{0 \ 1E-3 \ 0 \ 1\} \text{ m}$ (θ_z)₁ = (θ_z)₂ = 1-deg*

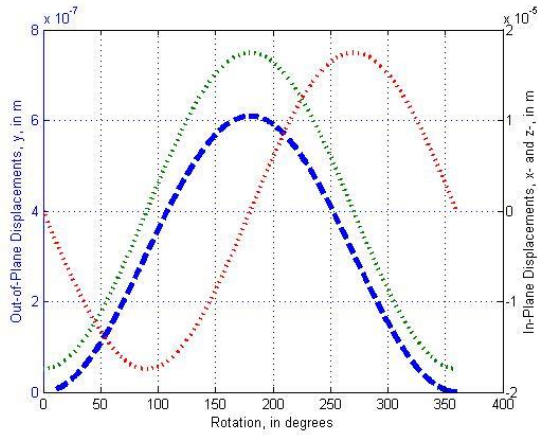
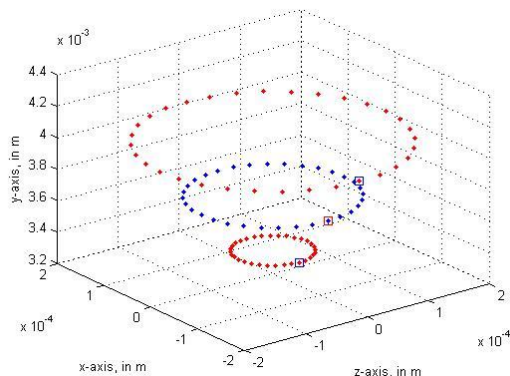
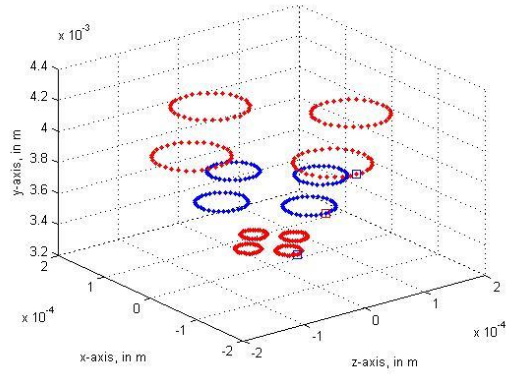


Figure 5. Double Circular-wedge Link System Out-of-plane and In-plane Displacements $(\theta_z)_1 = (\theta_z)_2 = 1\text{-deg}$

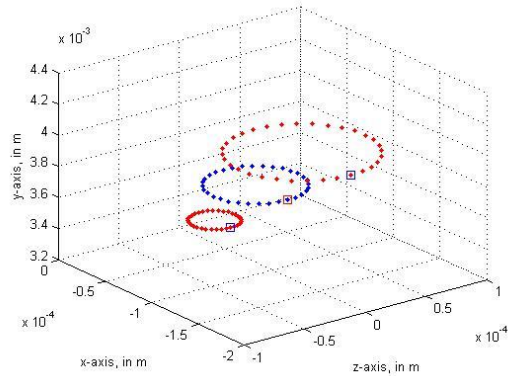
Figures 6(a)-6(d) are results that are parallel to those of Figures 4(a)-(d). They show the superposition of additional results when $\theta_{z1} = \theta_{z2}$ assumes values of 1-, 2- and 3-deg. The paths of the tip trajectories of P_L increasing in size with increasing circular-wedge angle. The significance of these graphs is to show that nanometric positioning along the y-axis is feasible, especially if the number of steps per revolution can be increased by an order of magnitude. This would require increasing the number of steps from 5-bits to 8- or more bits. The number of additional steps not only creates additional points in 3D-space but increases the resolution of these reachable points. In order to have control overreaching specified points in space, the inverse kinematics of this two-circular-wedge link system needs to be assessed, e.g., along a straight line, by the precise positioning of the stepping algorithm. The next section addresses the inverse kinematics of this two-circular-wedge link system.



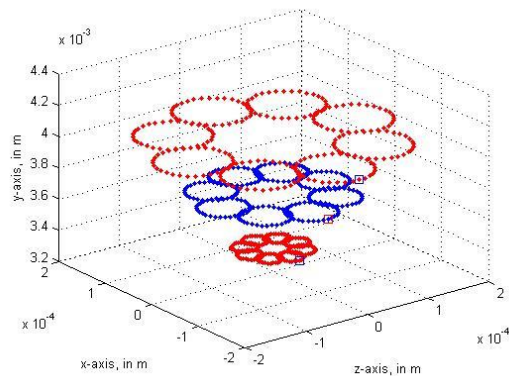
6(a) $(\theta_z)_1 = 1\text{-}, 2\text{-}$ and 3-degrees
Link 1 = 2^5 ; Link 2 = 2^0



6(c) Link 1 = 2^2 ; Link 2 = 2^5



6(b) Link 1 = 2^0 ; Link 2 = 2^5



6(d) Link 1 = 2^3 ; Link 2 = 2^5

Figure 6. Double Circular-wedge Link System Trajectory of a Point $P_L = \{0 \ 1E-3 \ 0 \ 1\} \text{ m}$ $(\theta_z)_1 = (\theta_z)_2 = 1\text{-deg}; 2\text{-deg}; 3\text{-deg}$

The Inverse Kinematics of the Double Circular-Wedge Link System

Equation 5 defines the forward kinematics problem for the double circular-wedge link system, i.e., given the position of a point on the positioner in a local frame of reference, it is possible to determine the position of that point at any and all possible positions determined by

the elements of the double circular-wedge link system in a global frame of reference. The inverse problem requires that for any identified point on the positioner in the global frame of reference, we be able to identify the precise orientations of the circular-wedges to arrive at said point.

Re-writing Equation 5, for ease of algebraic calculation, as follows

$$\mathbf{P}_G = RTR[\theta_{y_1}, h_1, \theta_{z_1}] RTR[\theta_{y_2}, h_2, \theta_{z_2}] \mathbf{P}_L. \quad (7)$$

We find that

$$RTR[\theta_{y_2}, h_2, \theta_{z_2}] = \begin{bmatrix} c\theta_{y_2}c\theta_{z_2} & -c\theta_{y_2}s\theta_{z_2} & s\theta_{y_2} & 0 \\ s\theta_{z_2} & c\theta_{z_2} & 0 & h_2 \\ -s\theta_{y_2}c\theta_{z_2} & s\theta_{y_2}s\theta_{z_2} & c\theta_{y_2} & 0 \\ 0 & 0 & 0 & 1 \end{bmatrix} \quad (8)$$

Which multiplied by $\mathbf{P}_L = \{0 \ L \ 0 \ 1\}^T$, yields

$$RTR[\theta_{y_2}, h_2, \theta_{z_2}] \mathbf{P}_L = \begin{bmatrix} c\theta_{y_2}c\theta_{z_2} & -c\theta_{y_2}s\theta_{z_2} & s\theta_{y_2} & 0 \\ s\theta_{z_2} & c\theta_{z_2} & 0 & h_2 \\ -s\theta_{y_2}c\theta_{z_2} & s\theta_{y_2}s\theta_{z_2} & c\theta_{y_2} & 0 \\ 0 & 0 & 0 & 1 \end{bmatrix} \begin{Bmatrix} 0 \\ L \\ 0 \\ 1 \end{Bmatrix} \quad (9)$$

or,

$$RTR[\theta_{y_2}, h_2, \theta_{z_2}] \mathbf{P}_L = \begin{Bmatrix} -L c\theta_{y_2}s\theta_{z_2} \\ L c\theta_{z_2} + h_2 \\ L s\theta_{y_2}s\theta_{z_2} \\ 1 \end{Bmatrix} \quad (10)$$

An equation similar to Equation 8 may also be written for *Link 1* as follows,

$$RTR[\theta_{y_1}, h_1, \theta_{z_1}] = \begin{bmatrix} c\theta_{y_1}c\theta_{z_1} & -c\theta_{y_1}s\theta_{z_1} & s\theta_{y_1} & 0 \\ s\theta_{z_1} & c\theta_{z_1} & 0 & h_1 \\ -s\theta_{y_1}c\theta_{z_1} & s\theta_{y_1}s\theta_{z_1} & c\theta_{y_1} & 0 \\ 0 & 0 & 0 & 1 \end{bmatrix} \quad (11)$$

to obtain the final equation for \mathbf{P}_G

$$\mathbf{P}_G = RTR[\theta_{y_1}, h_1, \theta_{z_1}] RTR[\theta_{y_2}, h_2, \theta_{z_2}] \mathbf{P}_L = \begin{Bmatrix} P_{G_x} \\ P_{G_y} \\ P_{G_z} \\ 1 \end{Bmatrix} \quad (12)$$

which results in,

$$\mathbf{P}_G = \begin{Bmatrix} P_{G_x} \\ P_{G_y} \\ P_{G_z} \\ 1 \end{Bmatrix} = \begin{Bmatrix} -A c\theta_{y_1} c\theta_{y_2} - (B + C) c\theta_{y_1} + D s\theta_{y_1} s\theta_{y_2} \\ -E c\theta_{y_2} + F \\ A s\theta_{y_1} c\theta_{y_2} + G s\theta_{y_1} + D c\theta_{y_1} s\theta_{y_2} \\ 1 \end{Bmatrix} \quad (13)$$

where the following terms define the geometry of the double circular-wedge link system and are taken as constants,

$$A = L c\theta_{z_1} s\theta_{z_2} \quad (14a)$$

$$B = L s\theta_{z_1} c\theta_{z_2} \quad (14b)$$

$$C = h_2 s\theta_{z_1} \quad (14c)$$

$$D = L s\theta_{z_2} \quad (14d)$$

$$E = L s\theta_{z_1} s\theta_{z_2} \quad (14e)$$

$$F = c\theta_{z_1} [L c\theta_{z_2} + h_2] + h_1 \quad (14f)$$

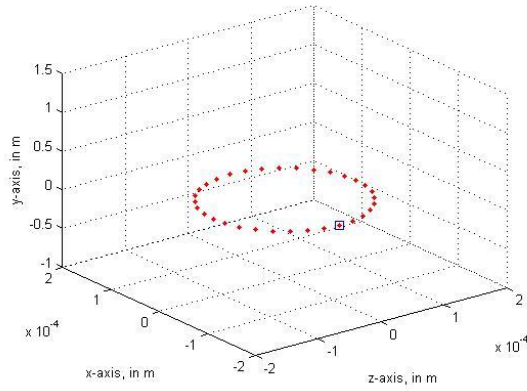
$$G = s\theta_{z_1} [L c\theta_{z_2} + h_2] \quad (14g)$$

The solution to the system of Equation 13 may be obtained: since the components of \mathbf{P}_G are known, subtracting the value of each component yields a nonlinear function whose roots may be found using a numerical solver. Appendix A shows a solution for θ_{y_2} from the equation for P_{G_y} using the *fzero* solver in Matlab®. This solution results in the value for θ_{y_2} , which then allows using either the nonlinear equation for P_{G_x} or for P_{G_z} to obtain a solution for θ_{y_1} . Substitution of these values in the forward kinematics equations allows reproduction of \mathbf{P}_G .

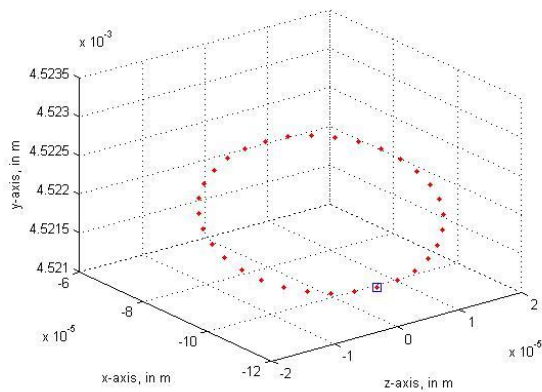
The Forward Kinematics of the Triple Circular-Wedge Link System

Equation (7) may easily be extended to add a third circular-wedge link to obtain,

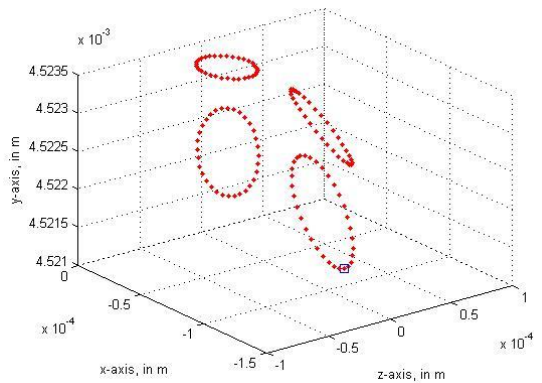
$$\mathbf{P}_G = RTR[\theta_{y_1}, h_1, \theta_{z_1}] RTR[\theta_{y_2}, h_2, \theta_{z_2}] RTR[\theta_{y_3}, h_3, \theta_{z_3}] \mathbf{P}_L = \begin{Bmatrix} P_{G_x} \\ P_{G_y} \\ P_{G_z} \\ 1 \end{Bmatrix} \quad (15)$$



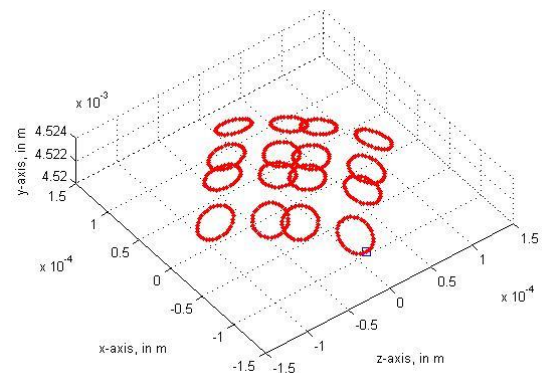
7(a) Link 1 = 2^5 ; Link 2 = 2^0 ; Link 3 = 2^0



7(b) Link 1 = 2^0 ; Link 2 = 2^0 ; Link 3 = 2^5



7(c) Link 1 = 2^0 ; Link 2 = 2^2 ; Link 3 = 2^5



7(d) Link 1 = 2^2 ; Link 2 = 2^2 ; Link 3 = 2^5

Figure 7. Triple Circular-wedge Link System Trajectory of a Point $P_L = \{0 \ 1E-3 \ 0 \ 1\}^T$ m $(\theta_z)_1 = (\theta_z)_2 = (\theta_z)_3 = 1\text{-deg}$

The Matlab® implementation of this equation leads to the results shown in Figure 7(a)-(d) for three circular-wedge links. The bottom, middle and top circular-wedge link are identified as Link 1 through Link 3, respectively. Figures 7(a) and 7(b) parallel the earlier results of Figure 4(a) and 4(b), respectively. Figure 7(a) shows the result of keeping the three circular-wedge links fixed relative to one another, while allowing for a 5-bit or 32-step stepping motion of the bottom circular-wedge link or Link 1.

Figure 7(b) is the result of keeping the bottom two circular-wedge links (Links 1 and 2) fixed relative to one another, while allowing for a 5-bit or 32-step stepping motion of the top circular-wedge link or Link 3.

Figure 7(c) keeps Link 1 static while allowing a 2-bit or 4-step stepping motion of Link 2 and allowing a 5-bit or 32-step stepping motion of the top circular-wedge link or Link 3.

Last, Figure 7(d) shows the path of the tip trajectories of P_L for a 2-bit or 8-step stepping motion of Links 1 and 2, and the 5-bit or 32-step stepping motion of Link 3.

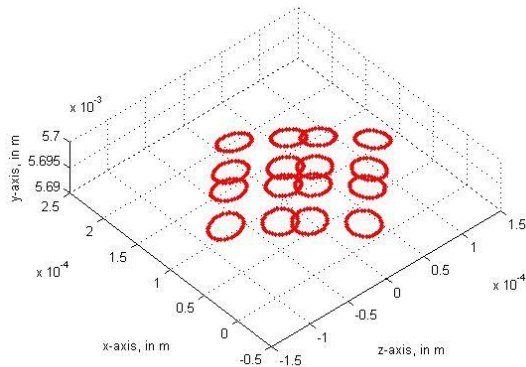
The Forward Kinematics of the Quadruple Circular-Wedge Link System

The further extension of Equation (15) to incorporation of a fourth circular-wedge link results in,

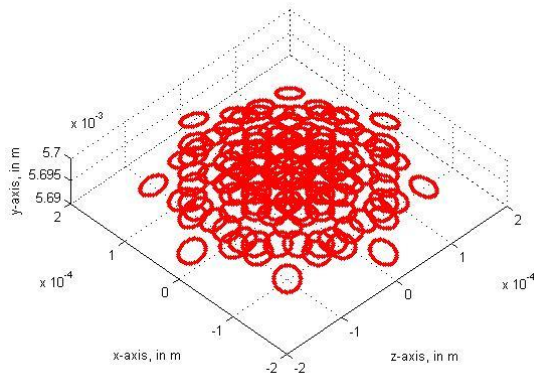
$$P_G = RTR[\theta_{y_1}, h_1, \theta_{z_1}] \dots RTR[\theta_{y_2}, h_2, \theta_{z_2}] RTR[\theta_{y_3}, h_3, \theta_{z_3}] \dots RTR[\theta_{y_4}, h_4, \theta_{z_4}] P_L = \begin{Bmatrix} P_{G_x} \\ P_{G_y} \\ P_{G_z} \\ 1 \end{Bmatrix} \quad (16)$$

The results are shown in Figures 8(a)-(d), where correspondingly the various circular-wedge links starting at the bottom are again numbered consecutively from 1 to 4. There is no particular reason as to the choice of number of steps to achieve the paths of the tip trajectories of P_L portrayed in Figures 8(a)-(d), except to point out that an increasing number of steps per circular-wedge link are used. For ease of reference we use the notation $[0 \ 2 \ 2 \ 5]$ to refer to the bits of stepping motion portrayed in Figure 8(a).

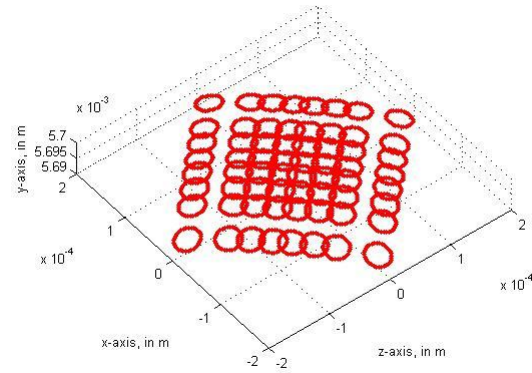
Similarly, the notation for Figures 8(b)-8(d) are [2 2 2 5], [3 2 2 5] and [4 2 2 5], respectively. The density of the points rapidly increases to allow a very high density of workspace coverage and redundancy.



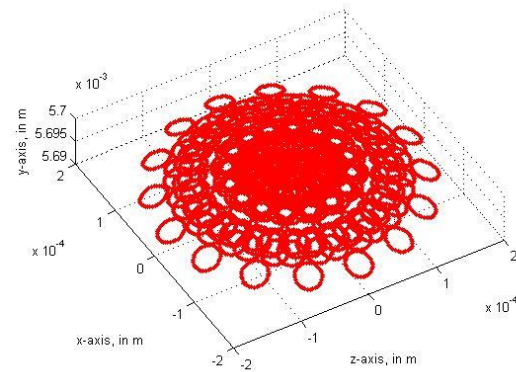
8(a) Link 1 = 2^0 ; Link 2 = 2^2 ; Link 3 = 2^2 ; Link 4 = 2^5



8(c) Link 1 = 2^3 ; Link 2 = 2^2 ; Link 3 = 2^2 ; Link 4 = 2^5



8(b) Link 1 = 2^2 ; Link 2 = 2^2 ; Link 3 = 2^2 ; Link 4 = 2^5



8(d) Link 1 = 2^4 ; Link 2 = 2^2 ; Link 3 = 2^2 ; Link 4 = 2^5

Figure 8. *Quadruple Circular-wedge Link System Trajectory of a Point $P_L = \{0 \text{ } 1\text{E-}3 \text{ } 0 \text{ } 1\} \text{ m}$ (θ_z)₁ = (θ_z)₂ = (θ_z)₃ = (θ_z)₄ = 1-deg*

The Nanometric Robotic Workspace

The main emphasis above has been to demonstrate the solution of the forward and inverse kinematics of the double circular-wedge link system to get a preliminary assessment of the potential for nanometric positioning. This section examines in greater detail whether or not that potential may be realized for the double circular-wedge link system.

The Double Circular-Wedge Link System

Table 1 summarizes the parameters associated with a double circular-wedge link system that have an impact on the size and characteristics of the system workspace, except for the Radius of the circular-wedge. The Radius of the circular wedge does not play a role in defining the workspace because the motion of the circular-

wedges is rotatory. This implies that the range of component sizes that the system design may incorporate for use as circular-wedges can be macroscopic, but depending on the application, microscopic circular-wedges may also be used. The potential for use of macroscopic components allows for the utilization of relatively large motors, gearing and other mechanical components in proof of concept designs.

Results

This section details achieving nanometric-capable motions with a double circular-wedge link system. Table 1 shows the parameters that are used in the calculations below. It is worth noting that the

dimensions of a typical $1.0E-2$ m radius circular-wedge with a dimension of its smallest circular-wedge height $h_0 = 1.0E-3$ m yields an opposite side dimension of $1.3491E-3$ m, which is reasonable from an additive manufacturing perspective.

Table 1.
Parameters that define a double circular-wedge link system

Parameters	Value
Number of Links	1, 2
Radius, R, in m	1.0E-2
Smallest Link Height, h_0 , in m	1.0E-3
Link 1 Angle, $(\theta_z)_1$, in degrees	0.5 & 1.0
Link 2 Angle, $(\theta_z)_2$, in degrees	0.5 & 1.0
Positioner Length, L, in m	1.0E-3
Positioner-Length Angle, θ , in degrees	0
Stepping Motion	0-bit to 10-bit

The preliminary calculations portrayed in Figure 4(b) for $\theta_{z1} = \theta_{z2} = 1.0$ deg, show that the tip of P_L describes a circular trajectory with a radius of about $1.7452E-5$ m in a plane at an inclination of 1-deg from the xz -plane. The separation between points is

$3.4213E-6$ m, showing the potential for achieving nanometric positioning. For example, an 8-bit or 256-step per revolution stepper motor achieves a separation between points of $4.2834E-7$ m, or 428.34 nm.

The calculations for the results portrayed in Figure 4(d) for a [3 8] (Link 1 = 2^3 ; Link 2 = 2^8) double circular-wedge link system is summarized in Table 2. Table 2 shows the range of motion that may be achieved, in the x-, z- and y- directions, for circular-wedge link angle $\theta_{z1} = 0.5$ and 1.0 deg; with link angle ratio that varies three orders of magnitude from 0.1 to 10, for each of these circular-wedge link angles. The calculations highlighted in yellow for $\theta_{z1} = \theta_{z2} = 1.0$ deg, i.e., for a link angle ratio of 1, show that the range of motion in the x- and z-directions is $1.1080E-4$ m, while the range in the y-direction is $6.0612E-6$ m, which is approximately three orders of magnitude less. Thus, the motion of the tip of P_L describes a relatively flat workspace in which the xz -plane motion is approximately 3-orders of magnitude greater than the out-of-plane motion. The out-of-plane motion shown in Figure 4(d) is shown exaggerated due to the choice of units that are different from the x- and z-axes. The same general observations hold for link angle ratios of 0.1 and 10.

Table 2.
Calculations for a double circular-wedge link system Link 1 = 2^3 ; Link 2 = 2^5

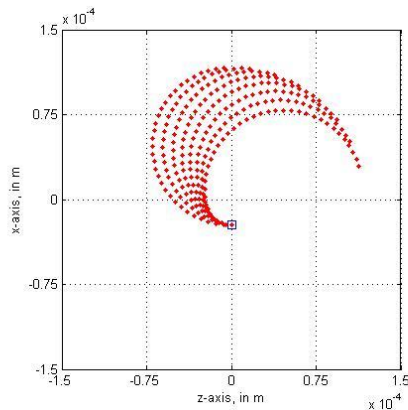
Link Angle, $(\theta_z)_1$	Link Angle Ratio, R = $(\theta_z)_2 / (\theta_z)_1$	$x_{min} = z_{min}$, in m	$x_{max} = z_{max}$, in m	$\Delta x = \Delta z$, in m	y_{max} , in m	y_{min} , in m	Δy , in m
0.5	0.1	-1.8402E-05	1.8402E-05	3.6804E-05	3.0959E-03	3.0959E-03	1.5230E-08
	1	-2.6940E-05	2.6940E-05	5.3881E-05	3.1743E-03	3.1745E-03	1.5230E-07
	10	-1.1221E-04	1.1221E-04	2.2441E-04	3.9575E-03	3.9590E-03	1.5211E-06
1.0	0.1	-3.6954E-05	3.6954E-05	7.3909E-05	3.1917E-03	3.1917E-03	6.0920E-08
	1	-5.5398E-05	5.5398E-05	1.1080E-04	3.3483E-03	3.3489E-03	6.0917E-07
	10	-2.3903E-04	2.3903E-04	4.7807E-04	4.9190E-03	4.9251E-03	6.0612E-06

Table 3.
Calculations for a double circular-wedge link system considering 8-bit stepping capability Link 1 = 2^3 ; Link 2 = 2^5

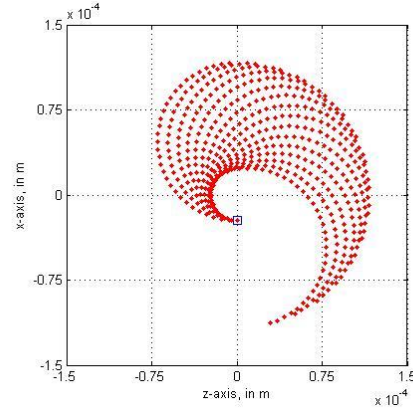
Link Angle, $(\theta_z)_1$	Link Angle Ratio, R = $(\theta_z)_2 / (\theta_z)_1$	$\Delta x = \Delta z$, in m	Δx / bit, in m	Δy , in m	Δy / bit, in m
0.5	0.1	3.6804E-05	1.4376E-07	1.5230E-08	5.9492E-11
	1	5.3881E-05	2.1047E-07	1.5230E-07	5.9492E-10
	10	2.2441E-04	8.7662E-07	1.5211E-06	5.9420E-09
1.0	0.1	7.3909E-05	2.8871E-07	6.0920E-08	2.3797E-10
	1	1.1080E-04	4.3280E-07	6.0917E-07	2.3796E-09
	10	4.7807E-04	1.8675E-06	6.0612E-06	2.3676E-08

Table 3 includes the same highlighted data as Table 2 but normalized to the number of steps achievable with an 8-bit stepper motor. Singling out the highlighted portion of Table 3, the per step resolution is $4.3280E-7$ m in the xz -plane and $2.3796E-9$ m in the out-of-plane or y -direction. Similar general observations hold for link angle ratios of 0.1 and 10. If this double circular-wedge link system is used as a means to push and retrieve an object only in the y -direction, the capability of nanometric resolution is easily achievable, with great precision in per step resolution.

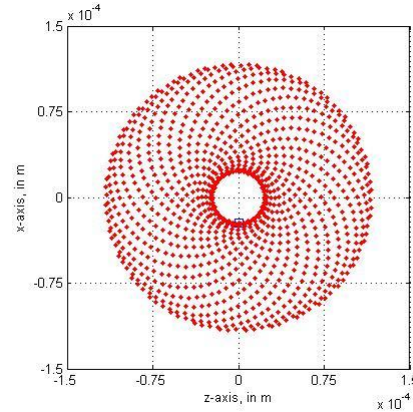
Figure 9(a)-(d) shows the results for a double circular-wedge link system with $\theta_{z_1} = 1.0$ deg and $\theta_{z_2} = 4.0$ deg, or a link angle ratio of 4. This arrangement is for a workspace density of $2^5 \times 2^6$ or 2,048 steps in the xz -plane utilizing a 5-bit and 6-bit stepper motor driving, the bottom and top circular-wedge links, respectively. The maximum y -displacement from the lowest to highest point is $2.4290E-6$ m. Figure 9(a) shows the result of only allowing the bottom link or Link 1 to move through $2^5/4 = 8$ of its possible steps; while the top link or Link 2 is allowed only $2^6/2 = 32$ of its steps, allowing Link 2 to describe only a semi-circular path. The end result is the superposition of 8 semi-circles that are offset from each other. Figure 9(b) shows the result of superposing 16 semi-circles. Finally, Figures 9(c) and 9(d) show the result of the superposition of 32 semi-circles in 2D and 3D, respectively. The versatility of this type of robotic arrangement is apparent from these graphs. Potentially, for an 8-bit stepper motor driving each of the links it would be possible to populate the workspace with 65,536 points.



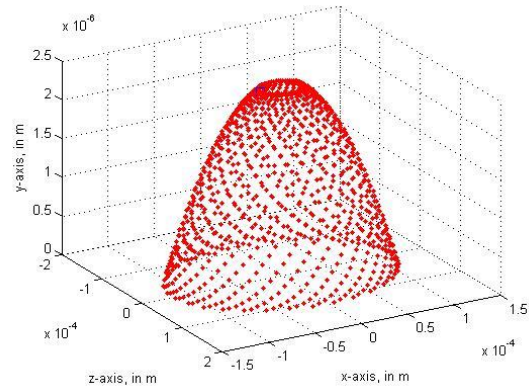
9(a) Link 1 = $2^5/4$; Link 2 = $2^6/2$



9(b) Link 1 = $2^5/2$; Link 2 = $2^6/2$



9(c) Link 1 = 2^5 ; Link 2 = $2^6/2$



9(d) Link 1 = 2^5 ; Link 2 = $2^6/2$

Figure 9. Double Circular-wedge Link System Trajectory of a Point $P_L = \{0 \ 1E-3 \ 0 \ 1\}$ m ($\theta_{z_1} = 1$ -deg; ($\theta_{z_2} = 4$ -deg

Summary and Conclusions

The use of several circular wedges to configure a robotic manipulator is a non-obvious arrangement of

elements that allows for versatility and flexibility in positioning. Additionally, it has the potential, when

using stepper motors, for repeatable, accurate and precise motion. Also, depending on the parameters that define the basic structure of the modular circular-wedges, the motion that is obtainable ranges from the macrometric to the nanometric scale. The main objective of this paper has been to explore the feasibility of using macro-scale circular-wedge links to achieve nano-metric positioning. The forward and inverse problems of using a double circular-wedge link system has been explored, as well

as a preliminary look at systems that involve three and four circular-wedge links. What is apparent from the various implemented simulations is that the workspace that is defined is in general planar. The achievable planar motion is several orders of magnitude greater than the out-of-plane motion. The details of actual implementation of a system is left for future work.

References

- Bejczy, A. (1975). Distribution of Control Decisions in Remote Manipulation. *1975 IEEE Conference on Decision and Control including the 14th Symposium on Adaptive Processes*, 14, 81-91.
doi:10.1109/CDC.1975.270654
- Cardenas-Garcia, J. F., & Preidikman, S. (2005). On Systems Of Circular Wedges For Serpentine Robots Applications. *Paper presented at the Conferencia de Mecánica Computacional, Buenos Aires, Argentina*.
- Cárdenas-García, J. F., Suryanarayan, K. P., & Ingalls, W. E. (1999). Mechanical Alignment Using Duplicate Circular Wedges. *Journal of Mechanical Design*, 121(2), 305-309.
<https://doi.org/10.1115/1.2829458>
- Denavit, J., & Hartenberg, R. S. (1955). A Kinematic Notation for Lower-Pair Mechanisms Based on Matrices. *ASME Journal of Applied Mechanics*, 22(2), 215-221.
- Gutkowski, L. J., & Kinzel, G. L. (1995). Kinematic Transformation Matrices for 3D Surface Contact Joints. *Journal of Mechanical Design*, 117(2A), 278-285.
<https://doi.org/10.1115/1.2826135>
- Harwood, O. P. (1973). *Huntington Beach*, CA Patent No. 3,712,481.
- Hirose, S. (1993). *Biologically Inspired Robots - Snake-like Locomotors and Manipulators*. New York, NY: Oxford University Press.
- Kucuk, S., & Bingul, Z. (2006). Robot Kinematics: Forward and Inverse Kinematics. In S. Cubero (Ed.), *Industrial Robotics: Theory, Modelling and Control* (pp. 117-148): Pro Literatur Verlag, Germany / ARS, Austria.
- McKerrow, P. J. (1991). *Introduction to Robotics*. Reading, MA: Addison-Wesley Publishing Co., Inc.

Appendix A

Matlab® Code to find the roots of a nonlinear function

```
% Read in needed data
%
[n,k,L,thetaZ1,thetaZ2,p2,height1,height2] = data;
% Calculation of angles in radians
%
thetaZ1 = thetaZ1*pi/180; thetaZ2 = thetaZ2*pi/180;
% Calculation of needed constants
%
A = L*cos(thetaZ1)*sin(thetaZ2);
B = L*sin(thetaZ1)*cos(thetaZ2);
C = height2*sin(thetaZ1); D = L*sin(thetaZ2);
E = L*sin(thetaZ1)*sin(thetaZ2);
F = cos(thetaZ1)*(L*cos(thetaZ2) + height2) + height1;
```



```

G = sin(thetaZ1)*(L*cos(thetaZ2) + height2);
% Calculation of randomly generated step for the TOP disk
%
j = fix(rand(1)*k); % TOP DISK
thetay2 = 180 + offsety2 - (j-1)*(360/(k-1));
% Calculation of randomly generated step for the TOP disk
%
i = fix(rand(1)*n); % BOTTOM DISK
thetay1 = 180 + offsety1 - (i-1)*(360/(n-1));
% Calculation of the Global Position of the point of interest
%
x1 = - cos(thetay1*pi/180)*cos(thetay2*pi/180)*A - ...      cos(thetay1*pi/180)*(B + C) ...
      + sin(thetay1*pi/180)*sin(thetay2*pi/180)*D;
y1 = - cos(thetay2*pi/180)*E + F;
z1 = sin(thetay1*pi/180)*cos(thetay2*pi/180)*A + ... sin(thetay1*pi/180)*G ...
      + cos(thetay1*pi/180)*sin(thetay2*pi/180)*D;
%
% Use of fzero - to obtain the Root of the nonlinear function %      for the y-component PG
%
f = @(x) [y1 + cos(x)*E - F];
yy = fzero(f,2); yyy = yy*180/pi;
% Comparison of assumed and calculated values
[thetay2 yyy]

```



Esta obra está bajo licencia internacional Creative Commons Reconocimiento-NoComercial 4.0.

En caso de que el artículo presentado sea aprobado para su publicación, los autores, mediante el documento “Declaración de originalidad y Cesión de derechos de autor”, transfieren a la revista los derechos patrimoniales que tienen sobre el trabajo para que se puedan realizar copias y distribución de los contenidos por cualquier medio y en acceso abierto, siempre que se mantenga el reconocimiento de sus autores y no se haga un uso comercial de la obra.